



Sulfoquinovosyldiacylglycerol and phosphatidylglycerol bilayers share biophysical properties and are good mutual substitutes in photosynthetic membranes

Stéphanie Bolik^{a,b}, Catherine Albrieux^a, Emanuel Schneck^c, Bruno Demé^{b,*}, Juliette Jouhet^{a,*}

^a Univ. Grenoble Alpes, CNRS, CEA, INRAE, IRIG, LPCV, 38000 Grenoble, France

^b Institut Laue-Langevin, 38000 Grenoble, France

^c Institute for Condensed Matter Physics, TU Darmstadt, 64289 Darmstadt, Germany

ARTICLE INFO

Keywords:

Sulfolipid
Phosphatidylglycerol
Neutron membrane diffraction
Phosphate starvation
Chloroplast

ABSTRACT

From cyanobacteria to higher plants, photosynthetic membranes are composed of two galactolipids, mono- and digalactosyldiacylglycerol (MGDG and DGDG, respectively), and two negatively charged lipids, sulfoquinovosyldiacylglycerol (SQDG) and phosphatidylglycerol (PG). In many environments, plants and algae grow in a shortage of nutrients, leading to the development of nutrient-saving mechanisms. For example, at the cellular level, in phosphate starvation, these mechanisms include conversion of phospholipids into phosphorus-free lipids. In photosynthetic membranes, PG is supposed to be replaced by SQDG in phosphate starvation whereas the opposite occurs in sulfur deprivation. All biological data confirm a complementary relationship between SQDG and PG and suggest the importance of maintaining the total amount of anionic lipids in photosynthetic membranes. Using neutron diffraction on reconstituted SQDG or PG lipid membranes, we demonstrate that, despite chemically different headgroups, PG and SQDG have similar physicochemical properties. With an equivalent diacylglycerol backbone, PG and SQDG membranes have a similar bilayer thickness and bending rigidity. They also have essentially the same response to hydration in terms of repulsion and interaction forces. The results presented here establish that SQDG and PG are good substitutes to each other in nutrient starvation conditions to maintain the chloroplast functional organization and its photosynthesis activity.

1. Introduction

Chloroplastic cells, where photosynthesis takes place, are composed by 80 % of non-phosphorus lipids, mostly galactolipids [1,2] but also the sulfolipid sulfoquinovosyldiacylglycerol (SQDG), which is synthesized and localized mainly in chloroplast membranes. Plastid membranes are also characterized by the presence of a phospholipid synthesized in the chloroplast envelope, phosphatidylglycerol (PG) [1,3]. In contrast, non-plastidial membranes are mainly composed of phospholipids that are synthesized in the endoplasmic reticulum (ER). Due to their immobility, plants take the nutrients directly from the soil in their environment. They are exposed to nutrient starvations, and therefore need to cope with the limitation of essential nutrients using adapted metabolisms. Phosphorus is one of the essential macronutrients for plant development, because it composes many molecules important for life, such as DNA and proteins, and because it is necessary for photosynthesis and

energy transfer [4–6].

Under phosphate (Pi) starvation, the strategy for plant cells is to improve Pi absorption, decrease Pi consumption and remobilize Pi reserves. It is well known that the lipid composition is strongly impacted in phosphate starvation with a phospholipid decline and a non-phosphorus lipid synthesis. Indeed, in plant cells, phospholipids constitute one third of Pi reserves [7], and in the ocean, phospholipid synthesis represents more than 18 % of the Pi taken up by the total planktonic community [8]. In plant cells, non-plastidial membrane phospholipids are replaced by the galactolipid DGDG (digalactosyldiacylglycerol) and the increase of DGDG synthesis is supposed to be related to an export of DGDG towards extraplastidial membranes and not to a change of the thylakoid galactolipid composition [9–11]. In algae, betaine lipids are synthesized to compensate the decrease of phospholipids [12,13]. In both organisms (plants and algae), when cultivated under Pi starvation, the level of PG in photosynthetic membranes decreases significantly. This decrease is

* Corresponding authors.

E-mail addresses: deme@ill.eu (B. Demé), juliette.jouhet@cea.fr (J. Jouhet).

<https://doi.org/10.1016/j.bbamem.2022.184037>

Received 9 April 2022; Received in revised form 22 June 2022; Accepted 22 August 2022

Available online 27 August 2022

0005-2736/© 2022 Elsevier B.V. All rights reserved.

compensated by an increase of the SQDG level [9,12,14–17]. In sulfur deprivation in *Chlamydomonas reinhardtii*, the opposite trend is observed with a decrease of SQDG and a remobilization of PG from the photosystem I [18,19].

SQDG is synthesized in the chloroplast from diacylglycerol (DAG) by the SQDG synthase (SQD2) adding a UDP-sulfoquinovose (uridine diphosphate-sulfoquinovose) with an α -link on position 3 (*sn*-3) of the glycerol motif [16,20]. PG is synthesized in the plastid, in the mitochondria, and in the ER. Phosphatidylglycerophosphate (PGP) synthase catalyzes the conversion of cytidine diphosphate-diacylglycerol and glycerol-3-phosphate to PGP, which is subsequently dephosphorylated to PG by PGP phosphatase [21]. Genes for PGP synthase have been well characterized, particularly in model organisms such as *Arabidopsis thaliana* [22] and genes responsible for the PGP phosphatase activity were recently identified by sequence similarity to the yeast [23]. In *Arabidopsis thaliana*, two homologs for PGP synthase have been identified: PGP1 and PGP2 [24]. PGP1 is dually targeted to plastids and mitochondria [25], whereas PGP2 is targeted to the ER [26]. In the *sqd2* mutant of *A. thaliana*, loss of SQDG was accompanied by an increase of PG content [20], reinforcing the idea that PG and SQDG are interchangeable.

Lipids contribute to the architecture and physical properties of membranes in terms of thickness, curvature, fluidity, and interactions. It is already known that PG and SQDG both self-organize in lamellar phase (L_α), a multilayer structure composed of parallel stacked bilayers [27,28]. At a given temperature, the membrane fluidity strongly depends on the fatty acid composition. The phase transition temperature indicates the transition between two states of the fatty acid chains: the gel phase, below the transition temperature, where fatty acids are solid (crystalline) and ordered, and the liquid phase, above the transition temperature, where fatty acids are fluid and disordered. The length and the unsaturation number in fatty acid chains modifies the transition temperature. In *A. thaliana*, SQDG and PG are rich in fatty acids 16:0 and 18:3. However, PG is the sole lipid that contains 16:1*t* (*trans*) [29]. Chilling-sensitive plants contain a high proportion of PG 16:0/16:0 and PG 16:0/16:1 *t*. The phase transition temperature of these two species is 42 and 32 °C respectively [30,31]. The phase transition temperature of SQDG 16:0/16:0 is 42 °C [30]. This indicates that with a similar fatty acid composition (16:0/16:0), but a distinguished polar head, PG and SQDG have a similar phase transition temperature. So far, PG and SQDG have been widely assumed to be interchangeable without any impact on membrane cell physiology, because they are both anionic, bilayer-forming lipids with similar transition temperature, and because they are located both in the plastids. However, to scrutinize this assumption, a deeper physicochemical characterization and comparison of these two lipids is required.

Neutron diffraction is a powerful and non-destructive technique that gives physical information on the membrane state, such as its organization, the bilayer and water layer thicknesses, the membrane interactions and the membrane bending rigidity. At physiological pH, the polar head of PG is negatively charged as the one of SQDG (Fig. 1), creating a repulsive electrostatic interaction between adjacent bilayers

[32,33]. The phosphate group and the sulfur trioxide carry the negative charge in PG and SQDG, respectively.

Experimental studies on the structure of SQDG bilayers are still lacking, but Coarse-Grained Molecular Dynamics (CGMD) simulation studies predicted the SQDG bilayer thickness to be around 44 Å [34,35]. In contrast, PG bilayers have been studied using both small angle X-ray and neutron scattering (SAXS and SANS) yielding a thickness of 35 Å for PG 16:0/16:0 (DPPG) [36,37], and 33.9 ± 1.1 Å for egg PG [38].

In this work, using neutron diffraction on PG and SQDG purified from plants, we show that the physicochemical properties of PG and SQDG are very similar. It is well known that PG is essential for photosynthesis and growth of all oxygenic phototrophs examined to date [39], whereas the requirement of SQDG for photosynthesis and growth varies with species [40]. Because a complementary relationship between SQDG and PG amount in thylakoid exists to maintain a constant amount of anionic lipids in membranes [22], our work gives proof to the hypothesis that SQDG is a good substituent for PG inside chloroplast membranes during phosphate starvation.

2. Materials and methods

2.1. Cultivation of *Arabidopsis thaliana* plants

Arabidopsis thaliana plants were first cultivated 15 days in long-day photoperiod (16 h light/8 h night) and then 4–5 weeks in short-day photoperiod (8 h light/16 h night) to produce maximum of leaves. The temperature was controlled at 22 °C during the day and 16 °C during the night. The quantity of light was 120 and 150 $\mu\text{mol}\cdot\text{m}^{-2}\cdot\text{s}^{-1}$, respectively for the long and short days. The hygrometry was fixed at 60 %. Leaves of plants were collected after 6 to 7 weeks of culture. They were immediately dropped in liquid nitrogen to be stored at -80 °C until further lipid extraction.

2.2. Lipid analysis

2.2.1. Lipid extraction

Leaves were lyophilized overnight. In liquid nitrogen, the frozen leaves were grind in powder, and transferred in an Erlenmeyer flask with 120 mL of boiled absolute ethanol during 5 min. Lipids were extracted according to Folch [41] adding 40 mL of methanol (MeOH) and 160 mL of chloroform (CHCl_3). The Erlenmeyer flask was saturated with argon, then closed and left for 1 h at room temperature on a stirrer. The lipid extract was filtered in a separatory funnel with ethanol washed quartz wool. To rinse the quartz wool, 60 mL $\text{CHCl}_3/\text{MeOH}$ 2/1 (v/v) were added. After the end of the filtration, 68 mL NaCl 1 % were added directly in the separatory funnel, and the solvents were mixed up under argon. Then, the separatory funnel was closed and left overnight for the formation of a biphasic. The organic phase (bottom phase) was collected and dried under argon in a warm water bath during around 3 h30. Lipids were transferred in Pyrex tubes using pure CHCl_3 . After solvent evaporation, lipids were stored at -20 °C.

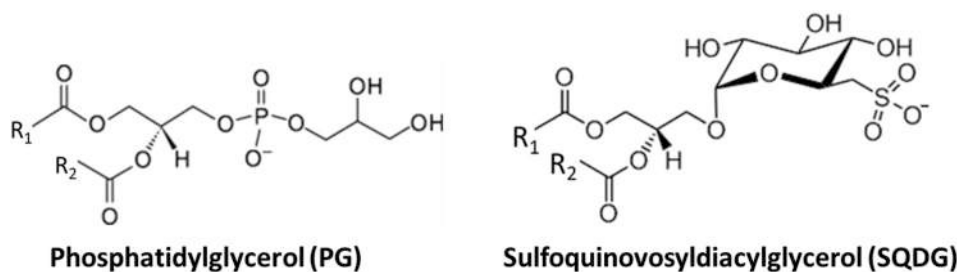


Fig. 1. Chemical structures of PG and SQDG. The phosphate or the sulfur trioxide groups carry the negative charge for PG and SQDG, respectively. The two fatty acid chains are denoted with R_1 and R_2 .

2.2.2. Lipid separation by thin layer chromatography (TLC)

1 mg of lipids was separated by two-dimensional thin layer chromatography (TLC) onto glass-backed silica gel plates (Merck). The first solvent was $\text{CHCl}_3/\text{MeOH}/\text{Water}$ 65/25/4 (v/v), and the second solvent was $\text{CHCl}_3/\text{Acetone}/\text{MeOH}/\text{Acetic Acid}/\text{Water}$ 50/20/10/10/5 (v/v). Lipids were visualized under UV light, after spraying with 2 % 8-anilino-1-naphthalenesulfonic acid in methanol. Each lipid class was scraped off the plate and lipids were extracted from the silica using the Bligh and Dyer method [42]. PG and SQDG were quantified by fatty acid methyl esters (FAMES) production and gas chromatography coupled to flame ionization detector (GC-FID) (Clarus 580, Perkin Elmer), or were analyzed by ion trap mass spectrometry (MS) (Amazon XL, Bruker) to validate their purity and determine the lipid molecules with their fatty acid position on the glycerol backbone, as described in [43].

2.3. Neutron diffraction experiments

Neutron diffraction data were collected at the D16 cold neutron diffractometer of the Institut Laue-Langevin (ILL, Grenoble, France). The experiments were repeated twice, with two sets of lipid extracts but with different water contrasts, either 100 % D2O or 8 % D2O. These measurements gave consistent results, but because only the 8 % D2O contrast is suited to disentangle the bilayer and water layer thicknesses [44], only this data set is presented here.

2.3.1. Sample preparation

Samples consisted of oriented lipid multilayer films (500 μg of dry material) spread from a 500 μL chloroform/methanol solution (1/2: v/v) on silicon wafers (3 in. diameter, 275 μm thick) from Si-Mat (Kaufering, Germany). Each wafer was cut to produce a rectangular shape of 20 mm (width) \times 75 mm (height). After lipid deposition, the solvent mixture was evaporated at room temperature and pressure until a solid film was obtained, and then dried 30 min under vacuum. The samples were then annealed at 25 $^{\circ}\text{C}$ in saturated D₂O vapor overnight, before transfer into a humidity chamber where the sample was equilibrated before the diffraction experiments.

2.3.2. Relative humidity control

Relative humidity (RH) scans at fixed sample temperature were performed *in situ* using the high-precision BerILL humidity chambers developed at ILL and described elsewhere [45]. The samples were mounted vertically on a manual 4-axis goniometer head (Huber, Germany) embedded in the humidity chamber and pre-aligned using a laser-based optical setup.

For both lipids, the temperature in the chamber was maintained at 25 $^{\circ}\text{C}$ during the measurements and the humidity was varied by changing the temperature of the water reservoir generating the water vapor. For each sample, the relative humidity was increased and monitored *in situ* step by step after each data collection of the previous RH condition, without opening the chamber at any time during the isothermal humidity scans.

Each sample was incubated in the humidity chamber prior to data collection. Since three identical chambers are available at ILL, two samples can be equilibrated while a third one is being measured. To reach 100 % RH at the end of the relative humidity ramping up, the chamber was taken out of the instrument and maintained overnight for further equilibrium at 100 %. The resulting range of humidities investigated was 30 % to 100 % RH. The error associated to the RH value was calculated using the errors of the temperature sensors of the sample and the reservoir bath, estimated to $\delta T_{\text{sample}} = \pm 0.05$ $^{\circ}\text{C}$ and $\delta T_{\text{res}} = \pm 0.05$ $^{\circ}\text{C}$. To each couple of temperatures corresponds a value of RH, and the standard deviation of the calculated RH is the error δRH .

Typical equilibrium times were ranging from 1 h at low humidity up to 3 h at high humidity. During this *in situ* equilibration phase, the position and intensity of the most intense Bragg reflections was monitored to ensure that for every condition (temperature, RH, and water contrast)

the sample was at equilibrium, a condition satisfied when constant d -spacing and constant intensity of Bragg reflections is observed.

The neutron scattering length density (NSLD) contrast between water and the lipid bilayers was obtained using $\text{H}_2\text{O}/\text{D}_2\text{O}$ ratios of 0:100 and 92:8 (v/v). Using the 8 % D₂O contrast lipid headgroups are highlighted thanks to the zero NSLD of water. From these profiles, the bilayer thickness can be directly extracted [44].

2.3.3. Osmotic pressure determination

The pressure Π applied to the membrane stacks by precise control of the humidity of the air in equilibrium with the sample, is calculated according to [46]:

$$\Pi = -\frac{k_b \times T_{\text{sample}}}{v_w^{\circ}} \times \ln\left(\frac{P}{P_0}\right) \quad (1)$$

where k_b is the Boltzmann constant ($k_b = 1.38.10^{-23}$ J.K $^{-1}$), T_{sample} , the sample temperature, v_w° the molecular volume of water (30 \AA^3) and P/P_0 the relative humidity RH.

2.3.4. Neutron diffraction instrument setup

D16 is a cold neutron diffractometer that uses a highly oriented pyrolytic graphite (HOPG) monochromator made of nine crystals whose orientation can be set to focus the beam vertically in a continuous manner from unfocused to detector or sample focusing. The wavelength of the neutron beam was $\lambda = 4.47$ \AA .

For membrane diffraction experiments, the graphite crystals are oriented in sample focusing geometry combined to a horizontal slit collimation to maximize the incident neutron flux at the sample (3×10^7 N.cm $^{-2}$.s $^{-1}$).

Fig. 2 shows the geometry of the experiment in top-view. The incident beam illuminates the sample plane with an adjustable angle of incidence Ω and is scattered into various directions at angles 2θ with respect to the incident beam. For each Ω , the 2θ -dependent intensity is recorded with a position-sensitive ^3He detector (MILAND) set to a distance of 950 mm from the sample. This 2D detector is made of 320 X by 320 Y wires spaced by 1 mm providing a pixel resolution of 1 mm \times 1 mm and a detection area of 320 \times 320 mm. By rotating the sample stage, and thus by stepwise variation of Ω , 2-dimensional maps of the intensity as a function of 2θ and Ω are recorded, as described previously [47,48]. These so-called “rocking curves” (Ω -scans) were collected by steps of 0.05 deg. in an Ω -range of -1 to 15 deg. In this procedure, the intensity is normalized to the detector pixels' sensitivity and solid angle, and to the illuminated sample area. The angles 2θ and Ω are associated with the reciprocal space coordinates q_z and $q_{||}$, i.e., the scattering vector components perpendicular and parallel to the sample plane, respectively, according to the geometrical relations (Fig. 2):

$$q_z = (2\pi/\lambda)[\sin(2\theta - \Omega) + \sin(\Omega)] \quad (2)$$

and

$$q_{||} = (2\pi/\lambda)[\cos(2\theta - \Omega) - \cos(\Omega)] \quad (3)$$

Fig. 2.C shows a typical intensity map, termed $I(2\theta, \Omega)$ in the following. It features the characteristic “Bragg sheets” of planar membrane multilayers [49]. The scattering intensity along the specular line ($\theta = \Omega$, $q_{||} = 0$) contains information on the structure perpendicular to the surface (notably the lamellar periodicity as encoded in the Bragg peak positions and the membrane scattering length density profile as encoded in the Bragg peak intensities). The diffuse scattering intensity ($\theta \neq \Omega$, $q_{||} \neq 0$) along the Bragg sheets additionally contains information on the in-plane structure, notably the membrane fluctuations in terms of their spatial self- and cross-correlation functions [47,49,50].

2.3.5. Data reduction

Sample rocking scans (Ω -scans) were analyzed using the ILL LAMP software [51]. Each detector frame resulting from an Ω step was

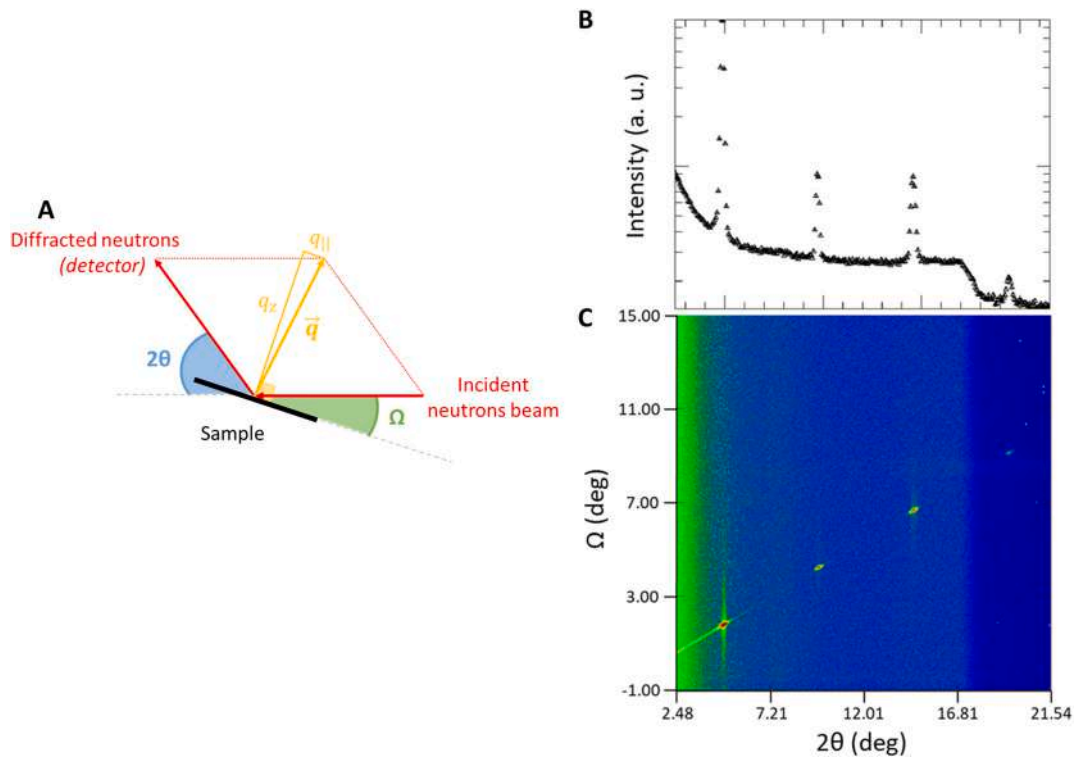


Fig. 2. A. Sample and beam geometries in top-view. The incident beam (red) illuminates the sample (black) with an adjustable angle of incidence Ω (green). For each Ω , the 2θ -dependent (blue) intensity is recorded by the detector. The angles 2θ and Ω are associated with the reciprocal space coordinates q_x and q_y (yellow). B. 1D integrated intensity measured for each Bragg peak. C. Reciprocal-space map resulting from a typical Ω -scan $I(2\theta, \Omega)$ showing the Bragg peak positions. (For interpretation of the references to colour in this figure legend, the reader is referred to the web version of this article.)

normalized to a detector calibration that accounts for the detector pixels' efficiency and solid angle. Then, each Ω step is reduced to 1D by vertical integration of the intensity in a ROI ($2\theta_y$ vs. $2\theta_x$ range) that corresponds to the location of Bragg peaks. Each Bragg peak position and intensity is fitted after summation of the intensity in an Ω range of 0.5 deg. (11 steps of 0.05 deg.) centered on the Bragg peak position. The peak shape of the fit to the data was Gaussian and a quadratic function was used for the background. Then, Bragg's law was used to determine the lamellar periodicity d according to:

$$2d\sin\theta_B = n\lambda \quad (4)$$

where θ_B is the half angle of the peak position $2\theta_B$, and λ the wavelength (4.47 Å). A linear fit to the plot $2\sin\theta$ vs. n , considering up to $n = 4$ orders, was used to obtain the d -spacing from the slope $s = \lambda/d$. The error on the d -spacing, δd , was given by propagating the error on the slope of the linear fit to the data.

2.3.6. Neutron scattering length density profiles

Neutron scattering length density profiles (NSLD) were calculated from the integrated intensities of Bragg peaks corrected for the neutron absorption (C_{abs}), and the Lorentz factor correction (C_{Lor}) according to [52], resulting in the corrected discrete structure factor of order n :

$$|F_n|^2 = C_{\text{abs}} C_{\text{Lor}} I_n \quad (5)$$

where I_n is the intensity of the Bragg peak at the order n .

The corrections are given by:

$$C_{\text{abs}} = \frac{\alpha}{1 - e^{-\alpha}}, \quad \alpha = \frac{2\mu t}{\sin\theta} \quad (6)$$

$$C_{\text{Lor}} = \sin(2\theta) \quad (7)$$

t is the sample thickness calculated from the deposited amount of dry

lipid (500 μg) and the sample area (15 cm^2). It is of the order of 10 μm before hydration, for a deposited amount of 1 mg, and scales linearly with the d -spacing as a result of hydration.

The NSLD were calculated using [53]:

$$\rho(z) = \frac{2}{d} \sum v_n F_n \cos\left(\frac{2\pi n z}{d}\right) \quad (8)$$

where z is the direction perpendicular to the bilayer planes and v_n corresponds to the phase of the structure factor. At the 8 % D_2O contrast, corresponding to the zero SLD of water, we tested different hypotheses for the discrete structure factor signs to obtain a centrosymmetric SLD profile with a minimum at $z = 0$, the bilayer mid-plane, where methyl groups are located and yield the highest density of hydrogens, and the maximum SLD for the polar head regions. The assigned phases that give the best agreement with these constraints were $-, -, +, -$ in agreement with [37].

We consider here as a definition of the bilayer thickness (d_b) the center-to-center distance between lipid polar heads as obtained from a fit to the two headgroup layer positions in the NSLD profile obtained according to Eq. (9) (as illustrated in Fig. S2). The error associated to d_b is given by the standard deviation between the fit and the calculated NSLD. Finally, the water layer thickness (d_w) is calculated from the known d -spacing and the bilayer thickness according to:

$$d_w = d - d_b \quad (10)$$

and the error is defined as $\delta d_w = \sqrt{\delta^2 d + \delta^2 d_b}$.

2.3.7. Bragg sheet analysis

According to the Discrete Smectic Hamiltonian description of interacting multilayers [54], the membrane fluctuation self and cross correlations that give rise to characteristic diffuse scattering are governed by the mechanical properties of the interacting membranes in terms of

the membrane bending modulus κ and the inter-membrane compression modulus B . As we have shown earlier, the reciprocal space maps obtained experimentally within this framework can be satisfactorily modeled solely based on the underlying mechanical parameters κ and B , and on an empirical cut-off parameter termed R [47]. In practice, this procedure relies on the kinematic approximation (KA) of wave scattering, because application of the more accurate distorted-wave Born approximation [50] would require detailed additional knowledge of the sample structure, which is unavailable. As a consequence, our KA-based treatment, which is only valid wherever the intensity is weak compared to the incident beam, does not correctly capture the specular maximum of the first Bragg sheet, where this condition is typically violated. In line with our more recent work [55], we therefore combine information from the first two Bragg sheets (Fig. S3): while the Caillé parameter:

$$\eta = \pi \kappa_B T / (2d^2 \sqrt{\kappa B/d}) \quad (13)$$

is obtained from the specular/diffuse scattering intensity ratio in the second Bragg sheet, the de Gennes parameter:

$$\Lambda = \sqrt{\kappa/(Bd)} \quad (14)$$

is obtained from the decay of the off-specular intensity in the first two Bragg sheets along $q_{||}$. The best-matching values of η , Λ , and R are then determined by their systematic variation in the model until the best agreement with the experimental data is achieved. Absorption close to $\Omega \approx 0$ and $\Omega \approx 2\theta$ was modeled as described previously [55]. Finally, the mechanical parameters are obtained by solving Eqs. (11) and (12) for κ and B .

3. Results

3.1. Fatty acid composition in PG and SQDG extracted from plant

Since the fatty acid composition of lipids likely affects their biophysical properties, we used natural thylakoid lipids to reflect more accurately the membrane characteristics and since the fatty acid composition of PG and SQDG is largely unaffected by phosphate starvation [56], we extracted them from Arabidopsis leaves grown on fertile soil. By ion trap mass spectrometry analysis, the fatty acid composition and the *sn*-1, *sn*-2 position of each fatty acid on the glycerol backbone have been determined (Fig. 3). PG and SQDG contain fatty acids with chain lengths of 16 and 18 carbons, with zero up to 3 unsaturations, corresponding to what is known in the literature for plant lipids [29,57]. In PG, the unsaturation on fatty acid 16:1 is in *trans*-conformation [58],

while the other unsaturations are in *cis*-conformation. This means, that the 16:1 *t* in PG looks like a 16:0 in terms of shape, because the *trans* unsaturation does not modify the chain orientation, compared to a *cis*-unsaturation that provides a rigid kink of 30° in the chain [59]. The presence of a C16 fatty acid in the *sn*-2 position of the glycerol backbone in the two lipids, is the signature of a lipid synthesis occurring inside the chloroplast (also called the “prokaryotic” pathway) [60,61].

Around 80 % of PG molecules are composed of 18:3/16:1 *t* and 18:3/16:0, both lipid molecules adopting an equivalent architecture. This is comparable to SQDG that is rich in 18:3/16:0 (around 50 %) and 18:2/16:0 (20 %), constituting around 70 % of the SQDG molecules. PG contains a double saturated specie 16:0/16:0, and its structural equivalent 16:0/16:1 *t*, both representing around 8 %, whereas SQDG has no unsaturated C16 species. SQDG contains also around 13 % of double unsaturated molecules (18:3/18:3) and small proportions of combinations of unsaturated C18 species that are not present in PG. However, whereas MGDG and DGDG are mainly composed of 18:3/18:3 or 18:3/16:3 molecules, it is not the case for SQDG where the fatty acid distribution is more similar to that of PG. Therefore, the fatty acid composition of these two natural lipids extracted from plants is similar and so, it should have little influence on the biophysical properties of membranes in comparison to the polar head differences.

3.2. Lamellar organization of PG and SQDG membranes

To investigate the mechanical properties of PG and SQDG membranes, lipids were spread at the surface of silicon wafers, and analyzed by neutron diffraction. As described in the materials and methods section, the relative humidity inside the chamber was controlled and changed during the experiment, starting at RH = 30 % to RH = 100 %, and the temperature of samples was maintained at 25 °C. Because PG 16:0/18:1 (POPG) has a melting temperature at −2 °C [62], we can suppose that at 25 °C, due to their fatty acid composition, our natural lipids are in fluid phase for all relative humidities throughout the whole experiment.

At RH = 30 %, samples are dehydrated, while at RH = 100 % samples are close to full hydration. During hydration, we followed the structural organization of membranes, the *d*-spacing and the modulation of Bragg peak intensities upon hydration. The diffraction data confirm that the two lipid types self-organize in lamellar phase as previously described in [27,28]. The presence of a high number of diffraction orders (up to 4) indicates that the bilayers were well correlated along the normal direction (regular *d*-spacing) (Fig. S1). PG and SQDG are not the main lipids in chloroplast membranes compared to the two galactolipids mono- and digalactosyldiacylglycerol (respectively MGDG and DGDG)

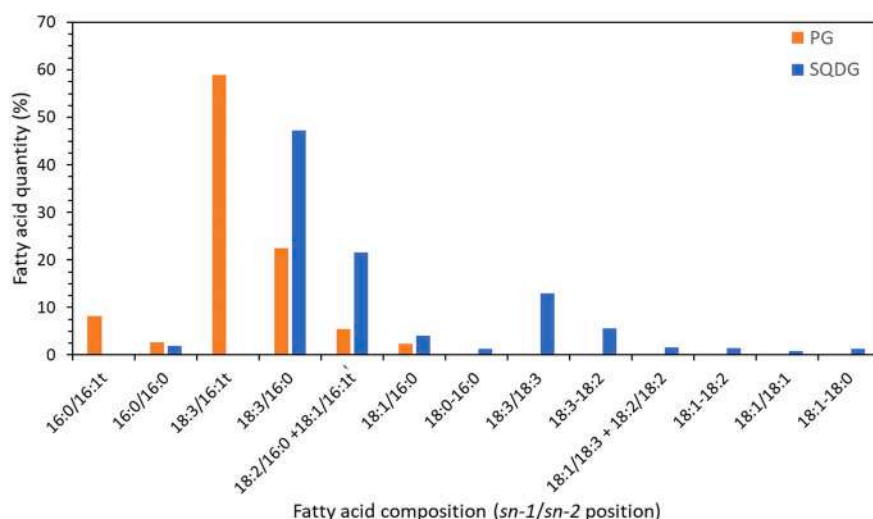


Fig. 3. Fatty acid composition and position (*sn*-1/*sn*-2) of PG and SQDG solved by ion trap type MS. PG (orange) contains a high portion of 18:3/16:1 *t* that is equivalent to 18:3/16:0, corresponding together to 80 % of the PG molecules, and a small portion of 16:0/16:1 *t*, 16:0/16:0 (10 %). SQDG (blue) contains a high portion of 18:3/16:0, 18:2/16:0, representing 70 % of the SQDG molecules, and a small portion of 18:3/18:3 (13 %) and all combinations of unsaturated C18 species. PG is the sole lipid of the thylakoid membranes containing a 16:1 *trans*-conformation. *The species 34:2 correspond to 18:2/16:0 in SQDG and 18:2/16:0 and 18:1/16:1 *t* in PG. (For interpretation of the references to colour in this figure legend, the reader is referred to the web version of this article.)

[3]. While DGDG also self-organizes in a lamellar phase, MGDG forms a hexagonal phase [32]. Therefore, MGDG contributes to the locally high curvature of thylakoids membranes, while DGDG, PG and SQDG are lipids that stabilize flat bilayer structures.

The lamellar d -spacing of PG and SQDG was measured at 8 % D₂O solvent contrast over the studied humidity range (Fig. 4). The results are presented in the form of pressure–distance curves, that is, plots of Π versus d . In our experimental conditions, because we worked under controlled vapor pressure, we could not explore the domain of very low osmotic pressure where repulsion falls off much more slowly and is dominated by electrostatic interactions [38].

For charged lipids at high pressure and at short range, there is clear evidence of an extra non-electrostatic repulsion that could be called “hydration force” [63,64]. However, here we will use the more generic term “short-range repulsion”. The humidity-dependent interaction pressure is found to exhibit an approximately exponential dependence on the lamellar period d (Fig. 4). We made an exponential fit to the data points from Fig. 4 with the following equation:

$$\pi = \pi_0 e^{-d/\lambda}$$

with λ representing a decay length as defined in [63]. The observed decay length λ of the lamellar period d includes short-range repulsions and membrane compression effects.

Here, we calculated $\lambda_{PG,d} = 4.5 \text{ \AA}$, and $\lambda_{SQDG,d} = 4.7 \text{ \AA}$, indicating that the decay of the forces exerted at short range between PG or SQDG bilayer are close to each other. This decay length is significantly higher than what could be observed for uncharged lipids such as phosphatidylcholine [63], indicating that electrostatic repulsion enhances the short-range repulsion. However, the interaction pressure and the membrane compression effects, represented by the decay length, act in the same way in PG and SQDG membranes. In [65], the authors found a decay length $\lambda = 11 \text{ \AA}$ for DPPG at pH = 7.2. For charged phospholipids, the decay length can be measured between 7 \AA and 13 \AA [65,66], that is higher than our result. Because we used extracted lipids from plants and not synthetic lipids and because we could observe in our mass spectrometry analysis some Na⁺ adduct of our lipids, maybe our lipid preparations contain some additional salts. This might explain the lower decay length observed in our experiment as compared to the one observed in the literature for synthetic PG.

3.3. Interaction pressures between PG and SQDG membranes

To disentangle the bilayer compression from the interaction forces between membranes, we need to estimate the decay length of the

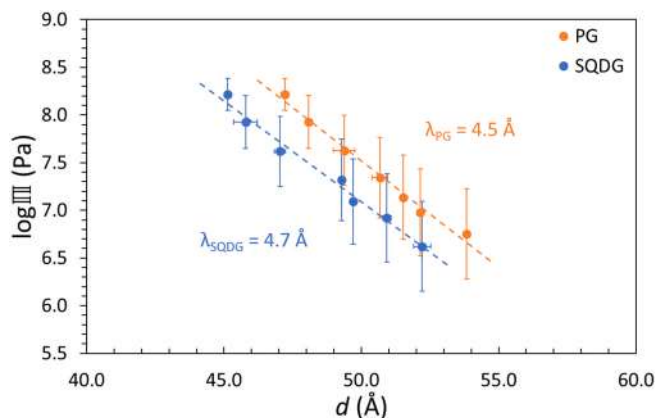


Fig. 4. Pressure–distance curves of PG (orange) and SQDG (blue) bilayer stacks at 25 °C with an 8 % D₂O contrast. The decay of the d -spacing is very similar for PG and SQDG bilayers. (For interpretation of the references to colour in this figure legend, the reader is referred to the web version of this article.)

hydration pressure versus the water layer thickness. Because experiments were performed at 8 % D₂O solvent contrast, that highlights the higher density headgroups [44], the calculated NSLD profiles give access to the bilayer and water layer thicknesses for the two lipids and at each investigated humidity (Fig. S2). The NSLD profiles are considered reliable if there is a minimum of 3 orders of diffraction in the neutron diffraction pattern and therefore could not be computed at the lowest humidity (RH = 30 %), where only 2 orders of diffraction are observed. In our NSLD profiles, the two peaks correspond to the middle of the polar head layers of a bilayer as described in [67]. Then we extracted the water layer thickness according to $d_w = d - d_b$ at each humidity for the two lipids (Fig. 5.A and B).

The results show that d_w increases exponentially with the same slope during swelling by 8 \AA in both PG and SQDG membranes. In addition, the decay length estimated at $\lambda_{PG,dw} = 6.4 \text{ \AA}$, and $\lambda_{SQDG,dw} = 7.2 \text{ \AA}$ are in the same range, confirming that the short-range repulsion is similar for PG and SQDG bilayers. In the literature, the decay length for PG is reported between 4.8 and 9.7 \AA [38], that is consistent with our results.

3.4. PG and SQDG bilayer thickness

For the two lipids, the decay lengths of the lamellar period and the water layer agree. We confirmed this result by plotting the pressure–membrane thickness curve (Fig. 5.B). Indeed, the bilayer thicknesses of PG and SQDG decrease with the increase of hydration, by around 2 \AA . The decrease of the bilayer thickness upon hydration is expected because the hydration favours disordering of the lipid components of the bilayer as previously reported for DOPC [68]. For PG, the bilayer thickness ranges from 36.8 to 35.7 \AA , in agreement with the bilayer thickness described in the literature, measured at $36.7 \pm 0.7 \text{ \AA}$ and 38.5 \AA in POPG membranes (PG 16:0/18:1) (respectively in [36,69,70]). For SQDG, the bilayer thickness decreases from 37.4 to 35.5 \AA , i.e. 1.9 \AA , slightly more than the PG bilayer thickness (1.1 \AA). We have no literature data for this lipid, only Coarse-Grained Molecular Dynamics (CGMD) simulations have been done on SQDG lipid. The bilayer thickness is calculated at 44 \AA [35] and 45 \AA [34] for fully saturated SQDG. These values obtained by simulations are higher than our experimental data, because they used fully saturated lipid chains that increase the fatty acid chain length, compared to a *cis*-unsaturated fatty acid that introduces angles in the carbon chain, and lead to its folding [71].

In our experiment, PG and SQDG bilayers essentially respond in the same way to hydration. Altogether, the bilayer thickness of PG and SQDG membranes is only slightly impacted by hydration, compared to the water layer thickness, meaning that hydration has a small impact on the bilayer compression, but has an influence on the swelling of water layers as already described for charged phospholipids [65].

As previously mentioned, PG and SQDG are two negatively charged lipids able to self-organize in lamellar phase and with this study, we show that the physical parameters are very similar. We also looked at the mechanical properties of bilayers, by analysing the off-specular intensity of the Bragg sheets at 100 % D₂O (Fig. S1). Fig. S3 shows the first two Bragg sheets obtained with PG and SQDG in D₂O atmosphere at 96 % RH. Plotted are the q_z -integrated Bragg sheet intensities as a function of Ω , featuring the respective central specular maxima symmetrically flanked by the slowly decaying diffuse scattering intensity. The latter is locally decorated with minima at conditions of high absorption ($\Omega \approx 0$ and $\Omega \approx 20$) and peaks arising from multiple scattering effects [55]. The solid lines superimposed to the experimental data points represent simulated Bragg sheet intensities corresponding to the best-matching parameters η and Λ in the continuum-mechanical model simultaneously describing the first and second Bragg sheets.

Two parameters can be extracted from this analysis, (1) the inter-membrane compression modulus B , and (2) the membrane bending modulus κ . The first one is a representation of the interactions between adjacent bilayers in a stack [67]. The higher the modulus B , the more strongly are the bilayers confined at a certain distance from their

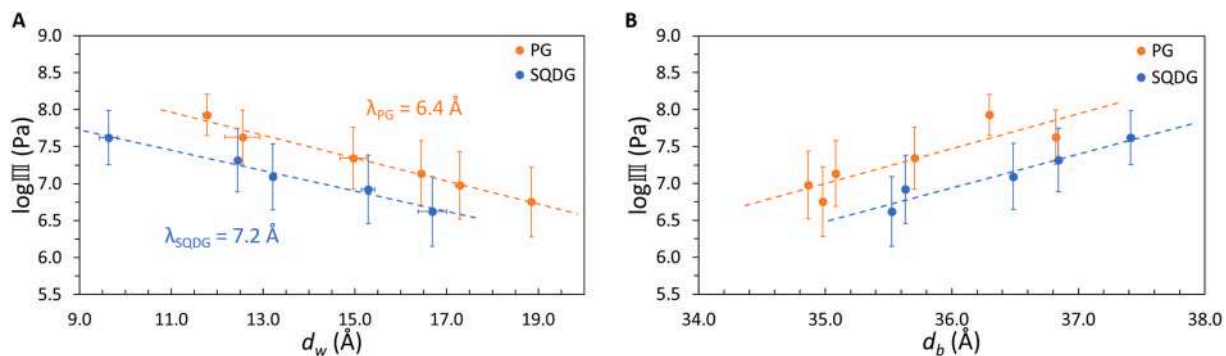


Fig. 5. Pressure-distance (d_w) (A) and pressure-membrane thickness (d_b) (B) curves of PG (orange) and SQDG (blue), measured at 25 °C. (For interpretation of the references to colour in this figure legend, the reader is referred to the web version of this article.)

neighbours due to interaction forces. The second modulus κ represents the energy required to bend a membrane from planarity to some defined curvature. As all previous results, the two parameters (κ and B) are very similar for the two membrane types. Indeed, the compression modulus B is obtained as 26 MPa and 32 MPa for PG and SQDG, respectively. Because the relative humidity was not exactly the same for the two lipids during experiment, the difference can be attributed to the higher hydration for SQDG than PG. Otherwise, the values are in the same order, demonstrating once again that the short-range interactions between PG and SQDG membranes are similar. The SQDG membrane bending rigidity (modulus κ) is found to be slightly higher than for PG membranes (4.1 and 2.8 $k_B T$, respectively). The difference can only be partially attributed to the slightly higher thickness of SQDG bilayers compared to PG bilayers ($\Delta d_b = 1.2$ Å), which according to classical theory of homogeneous beam would only result in a 10 % difference. The remaining difference must be attributed to slightly different in-plane compressibilities of the chemically different headgroup layer.

4. Discussion

The replacement of PG by SQDG in photosynthetic membranes under phosphate starvation conditions is well known. It has been described in microorganisms, such as the purple bacteria *R. sphaeroides* [14], diatoms and cyanobacteria [13,43,72,73], phytoplankton [74], but also in multicellular organisms, such as the plant model *Arabidopsis thaliana* [9]. In photosynthetic cells, PG and SQDG are not the main lipids in chloroplast membranes, where their biosynthesis occurs, and represent respectively around 9 and 6 % of chloroplast polar lipids in plants [75], and in *Chlamydomonas reinhardtii* [76]. However, *P. tricornutum* and *M. gaditana*, two secondary endosymbiont microalgae, are enriched in SQDG compared to green algae or land plants, with respectively around 20 and 11 % of total lipid composition [77]. In diatoms, the 3D structure of thylakoids inside the chloroplast is not the same as in plant chloroplasts [78,79], and could be explained by the specific lipid composition.

While the galactolipid MGDG forms the hexagonal II phase, the galactolipid DGDG and the anionic lipids PG and SQDG self-organize in lamellar phase. In the thylakoids structure, the ratio of MGDG and DGDG is very important to maintain lipid bilayers [32]. PG is also required for membrane organization in chloroplasts. Indeed, in PG-deficient *A. thaliana* mutants, the formation of large vesicles is induced inside the chloroplasts, leading to underdeveloped thylakoid membranes. This phenotype could be rescued in phosphate starvation conditions, where the SQDG content increases [80,81]. PG plays an important role in the photosynthesis activity, in particular in the electron transport [82], in the dimerization of the photosystem II (PSII) [83], for example. The loss of SQDG in SQDG-deficient *A. thaliana* mutant has no effect on the thylakoid architecture, but induces the PG synthesis to maintain a constant amount of total anionic lipids in membranes. During phosphate starvation, another anionic lipid, the

glucuronosyldiacylglycerol (GlcADG), is synthesized in chloroplast membranes [84] but it was found to be unable to complement the role of PG, particularly in photosynthesis [22], indicating that the presence of the negative charge is not sufficient to replace PG. However, in SQDG and PG-deficient mutant, grana stacking are reduced in *A. thaliana* leaf chloroplasts [17,22]. Altogether, it suggests that PG and SQDG are both important for photosynthetic membrane organization, which could explain why they are conserved in this membrane throughout the evolution. However, their biophysical properties are similar, suggesting that PG and SQDG should be interchangeable in phosphate starvation to maintain the thylakoid structure.

First of all, the fatty acid composition of PG and SQDG in *A. thaliana* is similar with a high amount of 18:3/16:0 or 18:3/16:1. However, SQDG contains a bit more than 15 % of 18:X/18:X species that are not present in PG. It is known that phospholipids with two polyunsaturated fatty acids make membranes highly permeable; whereas asymmetric saturated/polyunsaturated phospholipids provide low membrane permeability [85]. The fact that thylakoid membranes should prevent ion leakage to preserve the proton gradient to fuel the ATP synthase might explain why there is no PG containing 18:X/18:X species. No studies were done on the permeability of SQDG bilayers but according to the sugar lattice hypothesis, the H-bonds among glycosidic headgroups create a lipid domain fixed in space that could prevent membrane leakage [86,87]. In these conditions, like for MGDG and DGDG, the presence of SQDG with two polyunsaturated fatty acid would not be deleterious for photosynthetic membranes. Altogether, the presence of 18:X/18:X SQDG does not seem to affect PG replacement because the composition of SQDG is not modified during phosphate starvation [56].

The thickness of the diacylglycerol moiety is similar in the two lipids, leading to a similar hydrophobic bilayer thickness. In Fig. 5.B, the bilayer thickness of SQDG is 1.2 Å higher than that of PG. The small difference could be due to the polar head conformation. The PG head group conformation has been studied by single crystal analysis, and they showed that the phosphate group is located at ± 1.8 Å from the bilayer interface, and the charge carried by this phosphate is aligned in zigzag rows. The position of the glycerol head group attached to the phosphate group is alternately to the left and to the right from the phosphate rows [88]. Then, by single crystal analysis and molecular dynamics simulations, the orientation of PG polar headgroups has been found to be parallel to the membrane surface [88,89]. However, the conformation of the polar head of SQDG has not been described. Howard and Prestegard tried to solve it by NMR and molecular modeling and concluded that the head group of membrane-bound SQDG is reminiscent of that of DGDG and MGDG, the sugar group extends away from the bilayer surface permitting maximum hydration by water molecules [90]. In a previous study, Skarjune and Oldfield looked by NMR at the head group conformation of N-palmitoylglucosylceramide, that has a similar head group structure to that of SQDG. They concluded that the amplitude of fluctuations of the sugar moiety are large, always keeping

the carbohydrate head group extended from the bilayer to maximize hydrogen interactions with the bulk water [91]. This might explain why the SQDG bilayer is slightly thicker than a bilayer of PG with the same alkyl chains.

In our results, the water layer thickness between two bilayers of PG or SQDG increases with the hydration essentially in the same way (Fig. 5.A), the membrane thicknesses decrease with hydration in a similar way, too, and both membrane bending rigidity and the compression modulus are similar. This result suggests that the interaction forces, composed of hydration forces, electrostatic repulsion and bilayer compression forces, exerted on PG membranes are similar to that of SQDG membranes. All our results confirmed the hypothesis that SQDG is a good substitute for PG in membrane because they have similar physicochemical properties. This is not the case for all glycolipid/phospholipid replacements such as DGDG/PC as demonstrated previously [92].

5. Conclusions

Despite chemically different headgroups, PG and SQDG have similar properties with equivalent diacylglycerol backbone, equivalent bilayer and water thickness, and an equivalent response to hydration in terms of repulsion and interaction forces. The results presented here show that SQDG is a good substitute for PG in phosphate-deficiency conditions to maintain the functional organization of chloroplast membranes and, in turn, photosynthesis activity. However, in these experiments, we could not study the replacement of SQDG by PG within photosynthetic complexes where both lipids have been found to be present in crystallographic structures [83,93,94].

In future studies, it will be interesting to have access to the head group conformation to understand the character of the short-range repulsive forces. A key question will be the coupling between hydration forces and short-range electrostatic interactions. In our study, lipids are isolated from their natural environment, but in the cells, electrostatic screening by counter-ions takes place under different boundary conditions. For example, divalent cations such as Mg^{2+} are required for intracellular functions [95] and influence the membrane stacking in the stroma of chloroplasts [96]. Furthermore, in plant thylakoids, PG and SQDG are necessary to keep the stacked bilayer conformation, adding repulsion forces with their negative charges [32]. In algae, SQDG is more abundant than DGDG [43,77], and the thylakoid architecture is different from what is observed in plants [78,79]. It would be interesting to see if these two observations are related to each other.

Supplementary data to this article can be found online at <https://doi.org/10.1016/j.bbmem.2022.184037>.

Sample CRediT author statement

Stéphanie Bolik: Investigation, Writing- Original draft preparation
Catherine Albrieux: Resources
Emanuel Schneck: Investigation, Writing- Reviewing and Editing
Bruno Demé: Supervision, Writing- Reviewing and Editing
Juliette Jouhet: Supervision, Writing- Reviewing and Editing

Declaration of competing interest

The authors declare the following financial interests/personal relationships which may be considered as potential competing interests: Juliette Jouhet reports financial support was provided by French National Research Agency. Stéphanie Bolik reports financial support was provided by Institut Laue-Langevin. Stéphanie Bolik reports financial support was provided by French National Research Agency.

Data availability

I have shared the link to my data in the manuscript

Acknowledgments

The authors thank the Institut Laue-Langevin for the allocation of beamtime on the D16 diffractometer (<https://doi.org/10.5291/ILL-DA.TA.8-02-878> and <https://doi.org/10.5291/ILL-DATA.TEST-3119>) and for technical support. SB was supported by a joint funding by the ILL PhD Program and the French National Research Agency in the framework of the “Investissements d’avenir” program Glyco@Alps (ANR-15-IDEX-02) and the Labex GRAL, funded within the University Grenoble Alpes graduate school (Ecoles Universitaires de Recherche) CBH-EUR-GS (ANR-17-EURE-0003).

References

- [1] R. Douce, J. Joyard, Biochemistry and function of the plastid envelope, *Annu. Rev. Cell Biol.* 6 (1990) 173–216.
- [2] J. Joyard, E. Maréchal, M.A. Block, R. Douce, Plant galactolipids and sulfolipid Structure, distribution and biosynthesis, in: M. Smallwood, P. Knox, D.J. Bowles (Eds.), *Membranes: Specialized Function in Plants*, BIOS Scientific Publishers, Oxford, UK, 1996, pp. 179–194.
- [3] M.A. Block, A.-J. Dorne, J. Joyard, R. Douce, Preparation and characterization of membrane fractions enriched in outer and inner envelope membranes from spinach chloroplasts, in: C. Sybesma (Ed.), *Advances in Photosynthesis Research*, Springer, Netherlands, Dordrecht, 1984, pp. 27–30.
- [4] A. Carstensen, A. Herdean, S.B. Schmidt, A. Sharma, C. Spetea, M. Pribil, S. Husted, The impacts of phosphorus deficiency on the photosynthetic electron transport chain, *Plant Physiol.* 177 (2018) 271–284.
- [5] R. Thuynsma, A. Kleinert, J. Kossmann, A.J. Valentine, P.N. Hills, The effects of limiting phosphate on photosynthesis and growth of *Lotus japonicus*, *S. Afr. J. Bot.* 104 (2016) 244–248.
- [6] D. Wang, S. Lv, P. Jiang, Y. Li, Roles, regulation, and agricultural application of plant phosphate transporters, *Front. Plant Sci.* 8 (2017) 817.
- [7] Y. Poirier, S. Thoma, C. Somerville, J. Schiefelbein, in: A Mutant of *Arabidopsis* Deficient in Xylem Loading of Phosphate 97, 1991, p. 7.
- [8] B.A.S. Van Mooy, G. Rocap, H.F. Fredricks, C.T. Evans, A.H. Devol, Sulfolipids dramatically decrease phosphorus demand by picocyanobacteria in oligotrophic marine environments, *Proc. Natl. Acad. Sci.* 103 (2006) 8607–8612.
- [9] B. Essigmann, S. Guler, R.A. Narang, D. Linke, C. Benning, Phosphate availability affects the thylakoid lipid composition and the expression of SQD1, a gene required for sulfolipid biosynthesis in *Arabidopsis thaliana*, *Proc. Natl. Acad. Sci.* 95 (1998) 1950–1955.
- [10] H. Härtel, M. Peters-Kottig, C. Benning, The phospholipid-deficient *pho1* mutant of *Arabidopsis thaliana* is affected in the organization, but not in the light acclimation, of the thylakoid membrane, *Biochim. Biophys. Acta* 14 (1998).
- [11] J. Jouhet, E. Maréchal, B. Baldan, R. Bigny, J. Joyard, M.A. Block, Phosphate deprivation induces transfer of DGDG galactolipid from chloroplast to mitochondria, *J. Cell Biol.* 167 (2004) 863–874.
- [12] H. Murakami, T. Nobusawa, K. Hori, M. Shimojima, H. Ohta, Betaine lipid is crucial for adapting to low temperature and phosphate deficiency in nanochloropsis, *Plant Physiol.* 177 (2018) 181–193.
- [13] B.A.S. Van Mooy, H.F. Fredricks, B.E. Pedler, S.T. Dyhrman, D.M. Karl, M. Koblížek, M.W. Lomas, T.J. Mincer, L.R. Moore, T. Moutin, M.S. Rappé, E. A. Webb, Phytoplankton in the ocean use non-phosphorus lipids in response to phosphorus scarcity, *Nature* 458 (2009) 69–72.
- [14] C. Benning, J.T. Beatty, R.C. Prince, C.R. Somerville, The sulfolipid sulfoquinovosyldiacylglycerol is not required for photosynthetic electron transport in rhodospirillum rubrum but enhances growth under phosphate limitation, *Proc. Natl. Acad. Sci.* 90 (1993) 1561–1565.
- [15] N. Sato, Roles of the acidic lipids sulfoquinovosyl diacylglycerol and phosphatidylglycerol in photosynthesis: their specificity and evolution, *J. Plant Res.* 117 (2004) 495–505.
- [16] M. Shimojima, Biosynthesis and functions of the plant sulfolipid, *Prog. Lipid Res.* 50 (2011) 234–239.
- [17] B. Yu, C. Benning, Anionic lipids are required for chloroplast structure and function in *Arabidopsis*, *Plant J.* 36 (2003) 762–770.
- [18] K. Sugimoto, N. Sato, M. Tsuzuki, Utilization of a chloroplast membrane sulfolipid as a major internal sulfur source for protein synthesis in the early phase of sulfur starvation in *Chlamydomonas reinhardtii*, *FEBS Lett.* 581 (2007) 4519–4522.
- [19] K. Sugimoto, T. Midorikawa, M. Tsuzuki, N. Sato, Upregulation of PG synthesis on sulfur-starvation for PS I in *Chlamydomonas*, *Biochem. Biophys. Res. Commun.* 369 (2008) 660–665.
- [20] B. Yu, C. Xu, C. Benning, *Arabidopsis* disrupted in SQD2 encoding sulfolipid synthase is impaired in phosphate-limited growth, *Proc. Natl. Acad. Sci.* 99 (2002) 5732–5737.
- [21] C. Xu, B. Yu, A.J. Cornish, J.E. Froehlich, C. Benning, Phosphatidylglycerol biosynthesis in chloroplasts of *Arabidopsis* mutants deficient in acyl-ACP glycerol-3-phosphate acyltransferase, *Plant J.* 47 (2006) 296–309.
- [22] A. Yoshihara, N. Nagata, H. Wada, K. Kobayashi, Plastid anionic lipids are essential for the development of both photosynthetic and non-photosynthetic organs in *Arabidopsis thaliana*, *IJMS* 22 (2021) 4860.

- [23] Y. Zhou, G. Hölzl, K. vom Dorp, H. Peisker, M. Melzer, M. Frentzen, P. Dörmann, Identification and characterization of a plastidial phosphatidylglycerophosphate phosphatase in *Arabidopsis thaliana*, *Plant J.* 89 (2017) 221–234.
- [24] F. Müller, M. Frentzen, Phosphatidylglycerophosphate synthases from *Arabidopsis thaliana*, *FEBS Lett.* 509 (2001) 298–302.
- [25] E. Babychuk, F. Müller, H. Eubel, H.-P. Braun, M. Frentzen, S. Kushnir, *Arabidopsis* phosphatidylglycerophosphate synthase 1 is essential for chloroplast differentiation, but is dispensable for mitochondrial function: *arabidopsis* phosphatidylglycerophosphate synthase 1, *Plant J.* 33 (2003) 899–909.
- [26] R. Tanoue, M. Kobayashi, K. Katayama, N. Nagata, H. Wada, Phosphatidylglycerol biosynthesis is required for the development of embryos and normal membrane structures of chloroplasts and mitochondria in *arabidopsis*, *FEBS Lett.* 588 (2014) 1680–1685.
- [27] J.M. Seddon, Structure of the inverted hexagonal (HII) phase, and non-lamellar phase transitions of lipids, *biochimica et biophysica acta (BBA) - reviews on Biomembranes* 1031 (1990) 1–69.
- [28] G. Shipley, J.P. Green, B.W. Nichols, The phase behavior of monogalactosyl, digalactosyl, and sulfoquinovosyl diglycerides, *biochimica et biophysica acta (BBA) - Biomembranes* 311 (1973) 531–544.
- [29] J. Browse, L. Kunst, S. Anderson, S. Hugly, C. Somerville, A mutant of *arabidopsis* deficient in the chloroplast 16:1/18:1 desaturase, *Plant Physiol.* 90 (1989) 522–529.
- [30] D.G. Bishop, J.R. Kenrick, Thermal properties of 1-hexadecanoyl-2-trans-3-hexadecenoyl phosphatidylglycerol, *Phytochemistry* 26 (1987) 3065–3067.
- [31] N. Murata, J. Yamaya, Temperature-dependent phase behavior of phosphatidylglycerols from chilling-sensitive and chilling-resistant plants, *Plant Physiol.* 74 (1984) 1016–1024.
- [32] B. Demé, C. Cataye, M.A. Block, E. Maréchal, J. Jouhet, Contribution of galactoglycerolipids to the 3-dimensional architecture of thylakoids, *FASEB J.* 11 (2014).
- [33] K. Endo, K. Kobayashi, H. Wada, Sulfoquinovosyldiacylglycerol has an essential role in *thermosynechococcus elongatus* BP-1 under phosphate-deficient conditions, *Plant Cell Physiol.* 57 (2016) 2461–2471.
- [34] C.A. López, Z. Sovova, F.J. van Eerden, A.H. de Vries, S.J. Marrink, Martini force field parameters for glycolipids, *J. Chem. Theory Comput.* 9 (2013) 1694–1708.
- [35] C. Navarro-Retamal, A. Bremer, H.I. Ingólfsson, J. Alzate-Morales, J. Caballero, A. Thalhammer, W. González, D.K. Hincha, Folding and lipid composition determine membrane interaction of the disordered protein COR15A, *Biophys. J.* 115 (2018) 968–980.
- [36] J. Pan, D. Marquardt, F.A. Heberle, N. Kučerka, J. Katsaras, Revisiting the bilayer structures of fluid phase phosphatidylglycerol lipids: accounting for exchangeable hydrogens, *biochimica et biophysica acta (BBA) - Biomembranes* 1838 (2014) 2966–2969.
- [37] J. Pan, F.A. Heberle, J.R. Carmichael, J.F. Ankner, J. Katsaras, Time-of-flight bragg scattering from aligned stacks of lipid bilayers using the liquids reflectometer at the spallation neutron source, *J. Appl. Crystallogr.* 45 (2012) 1219–1227.
- [38] M.E. Loosley-Millman, R.P. Rand, V.A. Parsegian, Effects of monovalent ion binding and screening on measured electrostatic forces between charged phospholipid bilayers, *Biophys. J.* 40 (1982) 221–232.
- [39] K. Kobayashi, K. Endo, H. Wada, Roles of lipids in photosynthesis, in: Y. Nakamura, Y. Li-Beisson (Eds.), *Lipids in Plant and Algae Development*, Springer International Publishing, Cham, 2016, pp. 21–49.
- [40] K. Kobayashi, Role of membrane glycerolipids in photosynthesis, thylakoid biogenesis and chloroplast development, *J. Plant Res.* 129 (2016) 565–580.
- [41] J. Folch, M. Lees, G.H.S. Stanley, A simple method for the isolation and purification of total lipides from animal tissues, *J. Biol. Chem.* 226 (1957) 497–509.
- [42] E.G. Bligh, W.J. Dyer, A rapid method of total lipid extraction and purification, *Can. J. Biochem. Physiol.* 37 (1959) 911–917.
- [43] H. Abida, L.-J. Dolch, C. Mei, V. Villanova, M. Conte, M.A. Block, G. Finazzi, O. Bastien, L. Tirichine, C. Bowler, F. Rébeillé, D. Petroustos, J. Jouhet, E. Maréchal, Membrane glycerolipid remodeling triggered by nitrogen and phosphorus starvation in *Phaeodactylum tricornutum*, *Plant Physiol.* 167 (2015) 118–136.
- [44] M. Salvador-Castell, B. Demé, P. Oger, J. Peters, Structural characterization of an archaeal lipid bilayer as a function of hydration and temperature, *IJMS* 21 (2020) 1816.
- [45] J. Gonthier, M.A. Barrett, O. Aguetaz, S. Baudoin, E. Bourgeat-Lami, B. Demé, N. Grimm, T. Hauß, K. Kiefer, E. Lelièvre-Berna, A. Perkins, D. Wallacher, BerILL: the ultimate humidity chamber for neutron scattering, *JNR* 21 (2019) 65–76.
- [46] V.A. Parsegian, R.P. Rand, Interaction in membrane assemblies, in: *Handbook of Biological Physics*, Elsevier, 1995, pp. 643–690.
- [47] E. Schneck, B. Demé, C. Gege, M. Tanaka, Membrane adhesion via homophilic saccharide-saccharide interactions investigated by neutron scattering, *Biophys. J.* 100 (2011) 2151–2159.
- [48] E. Schneck, F. Rehfeldt, R.G. Oliveira, C. Gege, B. Demé, M. Tanaka, Modulation of intermembrane interaction and bending rigidity of biomembrane models via carbohydrates investigated by specular and off-specular neutron scattering, *Phys. Rev. E* 78 (2008), 061924.
- [49] T. Salditt, Thermal fluctuations and stability of solid-supported lipid membranes, *J. Phys. Condens. Matter* 17 (2005) R287–R314.
- [50] S.K. Sinha, E.B. Sirota, S. Garoff, H.B. Stanley, X-ray and neutron scattering from rough surfaces, *Phys. Rev. B* 38 (1988) 2297–2311.
- [51] D. Richard, M. Ferrand, G.J. Kearley, Analysis and visualisation of neutron-scattering data, *J. of Neutron Res.* 4 (1996) 33–39.
- [52] T.A. Harroun, J. Katsaras, S.R. Wassall, Cholesterol is found to reside in the center of a polyunsaturated lipid membrane, *Biochemistry* 47 (2008) 7090–7096.
- [53] D.L. Worcester, N.P. Franks, Structural analysis of hydrated egg lecithin and cholesterol bilayers II neutron diffraction, *J. Mol. Biol.* 100 (1976) 359–378.
- [54] N. Lei, C.R. Safinya, R.F. Bruinsma, Discrete harmonic model for stacked membranes: theory and experiment, *J. Phys. II France* 5 (1995) 1155–1163.
- [55] V.M. Latza, B. Demé, E. Schneck, Membrane adhesion via glycolipids occurs for abundant saccharide chemistries, *Biophys. J.* 118 (2020) 1602–1611.
- [56] H. Härtel, B. Essigmann, H. Lokstein, S. Hoffmann-Benning, M. Peters-Kottig, C. Benning, The phospholipid-deficient *pho1* mutant of *Arabidopsis thaliana* is affected in the organization, but not in the light acclimation, of the thylakoid membrane, *Biochim. Biophys. Acta* 1415 (1998) 205–218.
- [57] A. Burgos, J. Szymanski, B. Seiwer, T. Degenkolbe, M.A. Hannah, P. Gialvalisco, L. Willmitzer, Analysis of short-term changes in the *Arabidopsis thaliana* glycerolipidome in response to temperature and light: *arabidopsis* glycerolipids in abiotic stress, *Plant J.* 66 (2011) 656–668.
- [58] J. Dubacq, A. Tremolieres, Occurrence and function of phosphatidylglycerol Containing Delta-3-trans-hexadecenoic acid in photosynthetic lamellae, *Physiol. Veg.* 21 (1983) 293–312.
- [59] M.T. Hyvönen, T.T. Rantala, M. Ala-Korpela, Structure and dynamic properties of diunsaturated 1-palmitoyl-2-linoleoyl-sn-glycero-3-phosphatidylcholine lipid bilayer from molecular dynamics simulation, *Biophys. J.* 73 (1997) 2907–2923.
- [60] E. Heinz, P.G. Roughan, Similarities and differences in lipid metabolism of chloroplasts isolated from 18:3 and 16:3 plants, *Plant Physiology* 72 (1983) 7.
- [61] P.G. Roughan, R. Holland, C.R. Slack, The role of chloroplasts and microsomal fractions in polar-lipid synthesis from [1-14C]acetate by cell-free preparations from spinach (*Spinacia oleracea*) leaves, *Biochem. J.* 188 (1980) 17–24.
- [62] T. Wiedmann, A. Salmon, V. Wong, Phase behavior of mixtures of DPPC and POPG, *biochimica et biophysica acta (BBA) - lipids and lipidMetabolism* 1167 (1993) 114–120.
- [63] B. Kowalik, A. Schlaich, M. Kanduć, E. Schneck, R.R. Netz, Hydration repulsion difference between ordered and disordered membranes due to cancellation of membrane-membrane and water-mediated interactions, *J. Phys. Chem. Lett.* 8 (2017) 2869–2874.
- [64] R.P. Rand, V.A. Parsegian, Hydration forces between phospholipid bilayers, *biochimica et biophysica acta (BBA) - reviews on Biomembranes* 988 (1989) 351–376.
- [65] T.J. McIntosh, A.D. Magid, S.A. Simon, Interactions between charged, uncharged, and zwittionic bilayers containing phosphatidylglycerol, *Biophys. J.* 57 (1990) 1187–1197.
- [66] H.I. Petrache, S.W. Dodd, M.F. Brown, Area per lipid and acyl length distributions in fluid phosphatidylcholines determined by 2H NMR spectroscopy, *Biophys. J.* 79 (2000) 3172–3192.
- [67] J.F. Nagle, S. Tristram-Nagle, Structure of lipid bilayers, *biochimica et biophysica acta (BBA) - reviews on Biomembranes* 1469 (2000) 159–195.
- [68] S.S. Stachura, C.J. Malajczuk, E. Kuprusevicius, R.L. Mancera, Influence of bilayer size and number in multi-bilayer DOPC simulations at full and low hydration, *Langmuir* 35 (2019) 2399–2411.
- [69] N. Kučerka, M.-P. Nieh, J. Katsaras, Fluid phase lipid areas and bilayer thicknesses of commonly used phosphatidylcholines as a function of temperature, *biochimica et biophysica acta (BBA) - Biomembranes* 1808 (2011) 2761–2771.
- [70] G. Shahane, W. Ding, M. Palaokostas, M. Orsi, Physical properties of model biological lipid bilayers: insights from all-atom molecular dynamics simulations, *J. Mol. Model.* 25 (2019) 76.
- [71] M.X. Fernandes, M.A.R.B. Castanho, J. García de la Torre, Brownian dynamics simulation of the unsaturated lipid molecules oleic and docosahexaenoic acid confined in a cellular membrane, *Biochimica et Biophysica Acta (BBA) - Biomembranes* 1565 (2002) 29–35.
- [72] S. Güler, A. Seeliger, H. Härtel, G. Renger, C. Benning, A null mutant of *synechococcus* sp PCC7942 deficient in the sulfolipid sulfoquinovosyl diacylglycerol, *J. Biol. Chem.* 271 (1996) 7501–7507.
- [73] N. Sato, M. Hagio, H. Wada, M. Tsuzuki, Environmental effects on acidic lipids of thylakoid membranes, *Biochem. Soc. Trans.* 28 (2000) 912–914.
- [74] D.S. Maat, N.J. Bale, E.C. Hopmans, J.S. Sinninghe Damsté, S. Schouten, C.P. D. Brussaard, Increasing P limitation and viral infection impact lipid remodeling of the picophytoplankter *Micromonas pusilla*, *Biogeosciences* 13 (2016) 1667–1676.
- [75] M.A. Block, R. Douce, J. Joyard, N. Rolland, Chloroplast envelope membranes: a dynamic interface between plastids and the cytosol, *Photosynth. Res.* 92 (2007) 225–244.
- [76] L. Mendiola-Morgenthaler, W. Eichenberger, A. Boschetti, Isolation of chloroplast envelopes from *chlamydomonas* lipid and polypeptide composition, *Plant Sci.* 41 (1985) 97–104.
- [77] J. Jouhet, J. Lupette, O. Clerc, L. Magneschi, M. Bedhomme, S. Collin, S. Roy, E. Maréchal, F. Rébeillé, LC-MS/MS versus TLC plus GC methods: consistency of glycerolipid and fatty acid profiles in microalgae and higher plant cells and effect of a nitrogen starvation, *PLoS ONE* 12 (2017), e0182423.
- [78] S. Flori, P.-H. Jouneau, B. Bailleul, B. Gallet, L.F. Estrozi, C. Moriscot, O. Bastien, S. Eicke, A. Schober, C.R. Bártulos, E. Maréchal, P.G. Kroth, D. Petroustos, S. Zeeman, C. Breyton, G. Schoehn, D. Falconet, G. Finazzi, Plastid thylakoid architecture optimizes photosynthesis in diatoms, *Nat. Commun.* 8 (2017) 15885.
- [79] A.M. Pysznik, S.P. Gibbs, Immunocytochemical localization of photosystem I and the fucoxanthin-chlorophylla/c light-harvesting complex in the diatom *Phaeodactylum tricornutum*, *Protoplasma* 166 (1992) 208–217.
- [80] M. Hagio, I. Sakurai, S. Sato, T. Kato, S. Tabata, H. Wada, Phosphatidylglycerol is essential for the development of thylakoid membranes in *Arabidopsis thaliana*, *Plant Cell Physiol.* 43 (2002) 1456–1464.

- [81] K. Kobayashi, S. Fujii, M. Sato, K. Toyooka, H. Wada, Specific role of phosphatidylglycerol and functional overlaps with other thylakoid lipids in *Arabidopsis* chloroplast biogenesis, *Plant Cell Rep.* 34 (2015) 631–642.
- [82] B.R. Jordan, W.-S. Chow, A.J. Baker, The role of phospholipids in the molecular organisation of pea chloroplast membranes effect of phospholipid depletion on photosynthetic activities, *biochimica et biophysica acta (BBA) -Bioenergetics* 725 (1983) 77–86.
- [83] O. Kruse, B. Hankamer, C. Konczak, C. Gerle, E. Morris, A. Radunz, G.H. Schmid, J. Barber, Phosphatidylglycerol is involved in the dimerization of photosystem II, *J. Biol. Chem.* 275 (2000) 6509–6514.
- [84] Y. Okazaki, H. Otsuki, T. Narisawa, M. Kobayashi, S. Sawai, Y. Kamide, M. Kusano, T. Aoki, M.Y. Hirai, K. Saito, A new class of plant lipid is essential for protection against phosphorus depletion, *Nat. Commun.* 4 (2013) 1510.
- [85] M.M. Manni, M.L. Tiberti, S. Pagnotta, H. Barelli, R. Gautier, B. Antonny, Acyl chain asymmetry and polyunsaturation of brain phospholipids facilitate membrane vesiculation without leakage, *elife* 7 (2018), e34394.
- [86] M.Y. Yoshinaga, M.Y. Kellermann, D.L. Valentine, R.C. Valentine, Phospholipids and glycolipids mediate proton containment and circulation along the surface of energy-transducing membranes, *Prog. Lipid Res.* 64 (2016) 1–15.
- [87] M. Kanduć, A. Schlaich, A.H. de Vries, J. Jouhet, E. Maréchal, B. Demé, R.R. Netz, E. Schneck, Tight cohesion between glycolipid membranes results from balanced water-headgroup interactions, *Nat. Commun.* 8 (2017) 14899.
- [88] I. Pascher, S. Sundell, K. Harlos, H. Eibl, Conformation and packing properties of membrane lipids: the crystal structure of sodium dimyristoylphosphatidylglycerol, *biochimica et biophysica acta (BBA) -Biomembranes* 896 (1987) 77–88.
- [89] W. Zhao, T. Róg, A.A. Gurtovenko, I. Vattulainen, M. Karttunen, Atomic-scale structure and electrostatics of anionic palmitoyloleoylphosphatidylglycerol lipid bilayers with Na⁺ counterions, *Biophys. J.* 92 (2007) 1114–1124.
- [90] K.P. Howard, J.H. Prestegard, Conformation of sulfoquinovosyldiacylglycerol bound to a magnetically oriented membrane system, *Biophys. J.* 71 (1996) 2573–2582.
- [91] R. Skarjune, E. Oldfield, Physical studies of cell surface and cell membrane structure deuterium nuclear magnetic resonance studies of N-palmitoylglucosylceramide (cerebroside) head group structure, *Biochemistry* 21 (1982) 3154–3160.
- [92] M. Kanduć, A. Schlaich, A.H. de Vries, J. Jouhet, E. Maréchal, B. Demé, R.R. Netz, E. Schneck, Tight cohesion between glycolipid membranes results from balanced water-headgroup interactions, *Nat. Commun.* 8 (2017) 14899.
- [93] N. Mizusawa, H. Wada, The role of lipids in photosystem II, *Biochim. Biophys. Acta* 2012 (1817) 194–208.
- [94] H. Yu, T. Hamaguchi, Y. Nakajima, K. Kato, K. Kawakami, F. Akita, K. Yonekura, J.-R. Shen, Cryo-EM structure of monomeric photosystem II at 278 Å resolution reveals factors important for the formation of dimer, *Biochim. Biophys. Acta Bioenerg.* 1862 (2021), 148471.
- [95] A.-C. Pohland, D. Schneider, Mg²⁺ homeostasis and transport in cyanobacteria – at the crossroads of bacterial and chloroplast Mg²⁺ import, *Biol. Chem.* 400 (2019) 1289–1301.
- [96] I. Rumak, K. Gieczewska, B. Kierdaszuk, W.I. Gruszecki, A. Mostowska, R. Mazur, M. Garstka, 3-D modelling of chloroplast structure under (Mg²⁺) magnesium ion treatment relationship between thylakoid membrane arrangement and stacking, *biochimica et biophysica acta (BBA) -, Bioenergetics* 1797 (2010) 1736–1748.